Journal of Civil Engineering and Urban Planning (2025)
Clausius Scientific Press, Canada

DOI: 10.23977/jceup.2025.070119
ISSN 2616-3969 Vol. 7 Num. 1

Differential Effects of Soil-Structure Interaction on Seismometer Recordings

Shaobo Han*, Pengliang Ren

College of Architecture and Civil Engineering, Beijing University of Technology, Beijing, 100124, China
**Corresponding author*

Keywords: Soil-Structure Interaction; Seismometer; Integrated Finite Element Method; Spectral Analysis

Abstract: China is situated in a seismically active zone, necessitating urgent improvements in earthquake disaster prevention and mitigation capabilities. To address the distortion of seismic motion recordings caused by soil-structure interaction (SSI) in low-rise residential buildings equipped with seismometers, this study establishes an integrated finite element model of a soft soil site, shallow foundation, and three-story reinforced concrete frame structure based on seismometer deployment characteristics in the Ya'an region. Four real seismic ground motion records were selected for numerical simulations of vertically incident SV waves, comparing acceleration response differences between structural monitoring points and free-field surface conditions. Key findings include:(1) Acceleration peaks at structural foundations and lower-story wall monitoring points show minimal differences but significant deviations from free-field recordings, with masonry infill walls dominating low-story acceleration distribution;(2) SSI-induced amplification/attenuation effects on structural acceleration responses are modulated by seismic spectral characteristics, showing 1.25× amplification in the structural natural frequency range (0.2–0.6 s) and high-frequency attenuation (>15 Hz) due to soil filtering;(3) Acceleration response spectra exhibit notable enhancement within the structural characteristic period range (0.2–0.6 s), indicating selective amplification of short-period seismic motions by residential buildings;(4) Site flexibility exacerbates high-frequency filtering, while instrumental intensity deviations primarily arise from coupled seismic motion characteristics, structural parameters, and site conditions, with SSI alone contributing minimally to intensity assessment. These results provide theoretical foundations for optimizing seismometer deployment and revising earthquake early warning systems.

1. Introduction

China is situated at the intersection of the Pacific Ring of Fire and the Eurasian seismic belt, rendering it one of the most earthquake-prone countries with significant seismic hazards. Currently, China's earthquake disaster prevention and mitigation capabilities remain underdeveloped, making the effective defense against seismic threats and reduction of their destructive impacts a critical challenge for researchers and national authorities. Drawing on advanced international experiences

from Japan and the United States in earthquake early warning systems [1, 2], the National Earthquake Early Warning Project has established over 10,000 general stations equipped with MEMS accelerometers, achieving nationwide minute-level seismic intensity reporting. However, due to the requirements for high-density distribution and extensive coverage in station siting, seismometers are often installed in two- or three-story residential buildings [3]. The recordings from seismometers within low-rise structures may be distorted by structural influences, failing to objectively reflect free-field ground motions. To address this issue, scholars have investigated the effects of structural presence on indoor seismic recordings through the lens of soil-structure interaction (SSI).

The utilization of strong-motion data from existing stations to investigate soil-structure interaction (SSI) effects on seismic recordings represents a widely adopted methodology among international researchers. In 1983, Campbell [4] analyzed Imperial Valley earthquake data and found that horizontal motion amplitudes recorded within small masonry structures exceeded surface accelerometer measurements by 2–3 times near 10 Hz. Stewart [5] compared foundation and free-field acceleration data, identifying significant correlations between spectral acceleration discrepancies and foundation embedment ratio, dimensionless frequency, and structure-to-soil stiffness ratio. Shallow foundations exhibited low-frequency spectral accelerations approximating free-field motions, while deamplification effects were observed in horizontal peak acceleration and velocity at foundations.Pandey [6], based on 99 earthquake recordings from 22 shallow-founded buildings in California, demonstrated that differences between foundation and free-field motions could manifest as either reduction or amplification. Dimitris Sotiriadis [7–9] derived predictive expressions for foundation/free-field motion intensity indices through nonlinear regression analysis of extensive datasets, incorporating building characteristics and site conditions. Michail Ntinalexis [10] and Zhou Baofeng [11] investigated elevation-dependent time-frequency characteristics of strong-motion recordings via shake table tests.In numerical studies, Liang [12] employed the Indirect Boundary Element Method (IBEM) with non-singular Green’s functions to elucidate site effects in dynamic SSI. Subsequent work by Liang [13] combined finite element method (FEM) simulations for near-field soil with IBEM for far-field domains, further exploring soil nonlinearity impacts on SSI. Pitilakis [14] and Karapetrou [15] utilized two-dimensional soil-block models to assess SSI effects on reinforced concrete structures. Francesco Cavalieri [16] developed three-dimensional nonlinear soil-block models to quantify SSI influences on instrument recordings in light shed structures and large-scale buildings with basements.

The stochastic nature of earthquakes results in limited datasets containing both co-located building and adjacent free-field recordings. Furthermore, most existing recording stations are situated in basements of large-scale structures, leading to a scarcity of quantitative studies on low-rise shallow-founded buildings. Numerical simulation methods offer a viable and effective approach to address this gap, enabling parametric analysis through diverse modeling frameworks to investigate soil-structure interaction (SSI) under varying site conditions and structural conFigureurations. This study establishes an integrated finite element model of a soil-foundation-residential building system, reflecting potential seismometer deployment scenarios in typical residential structures. The model analyzes the influence of seismometer placement locations on seismic recordings under different ground motion inputs.

2. Computational Model and Input

2.1 Finite Element Modeling

Based on the typical residential building structural conFigureurations in the Ya'an region of Sichuan Province, a two-bay three-story reinforced concrete frame structure with masonry infill

walls was established, featuring a first-story height of 3.3 meters, upper-floor heights of 3.0 meters, a span of 4.2 meters, a longitudinal depth of 4.2 meters, and an overall plan dimension of 8.8 meters by 8.8 meters. The foundation, with a plan dimension of 10 meters by 10 meters and an embedment depth of 0.5 meters, was integrated into a soil domain measuring 50 meters by 50 meters horizontally and 20 meters vertically, designed to exceed five times the superstructure plan dimensions to mitigate boundary effects from viscoelastic dynamic artificial boundaries and seismic wave dissipation damping. The soil medium was discretized using a 1-meter mesh size, with detailed dimensional and material parameters provided in Table 1,

Table 1 Dimensions and Parameters of the Upper Structure Materials

Type	Dimension(mm)	Material	ρ(kg/m ³)	ν	E(Gpa)
Beam cross-section	400×200	C30 Concrete	2500	0.2	30
Column cross-section	400×400				
Thickness of the floor slab	100				
Thickness of the foundation	500				
Thickness of the infill wall	240	Masonry	1500	0.2	1.59

Due to the use of explicit analysis steps in ABAQUS for solving the integrated soil-structure model, the incorporation of solid reinforcement elements would significantly reduce computational efficiency; thus, this study adopts a homogenized approach to account for reinforced concrete material properties by dispersing steel reinforcement into concrete, with average reinforcement ratios of 1% for slabs and 4% for beams and columns. The three-dimensional finite element model of the soil-foundation-superstructure system developed in ABAQUS (Figure. 1) employs solid elements for all components, with the concrete foundation embedded into the soil medium to accurately simulate soil-structure interaction.

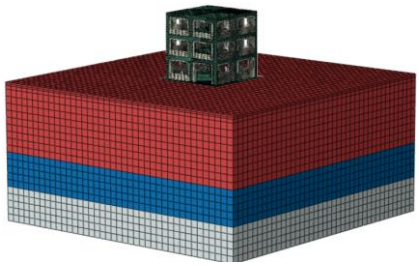

Figure 1: Finite Element Calculation Models of Different Upper Structures

Soil-foundation contact pairs were defined using a tangential penalty function with a friction coefficient of 0.3 and "hard" normal contact behavior allowing separation post-contact. Soil material properties (Table 2) include multilayered soft soil strata to replicate response variations of residential buildings on heterogeneous soft soil deposits, with three-dimensional viscoelastic artificial boundaries [17] applied to the soil domain's lateral and bottom surfaces to minimize wave reflection artifacts.

Table 2 Parameters of the Soil Materials

Layer	Type	Thickness(m)	E(Mpa)	ν	ρ(kg/m³)
1	Silty clay	10	93.8	0.33	1800
2	Silty clay	5	126	0.33	1850
3	Silty sand	5	202	0.33	1900

2.2 Seismic Input Selection

The selected ground motion inputs, as detailed in Table 3, include seismic records from the Kobe earthquake (Japan), Friuli earthquake (Italy), Imperial Valley earthquake (USA), Loma Prieta earthquake (USA), and Trinidad earthquake (USA). For each event, 15-second time windows centered on peak acceleration were extracted and applied as seismic inputs to the model, with a uniform time step of 0.01 s. This study exclusively considers vertically incident SV waves propagating upward from the model base, assuming plane-wave incidence to simulate idealized seismic wave propagation conditions.

Table 3: Information of the Input Seismic Ground Motions

Seismic Wave	Station	PGA(g)	Predominant Period(s)
Kobe (Japan)	KAKOGAWA(CUE90)	0.3447	0.16
Friuli (Italy)	TOLMEZZO(000)	0.3513	0.26
The Loma Prieta (USA)	090 CDMG STATION 47381	0.3674	0.22
The Trinidad (USA)	090 CDMG STATION 1498	0.1936	0.28

The acceleration time-history curves, acceleration response spectra, and acceleration Fourier spectra of the four seismic ground motions are shown in Figure. 2, with their energy predominantly concentrated near the structural fundamental frequency in the simulated model.

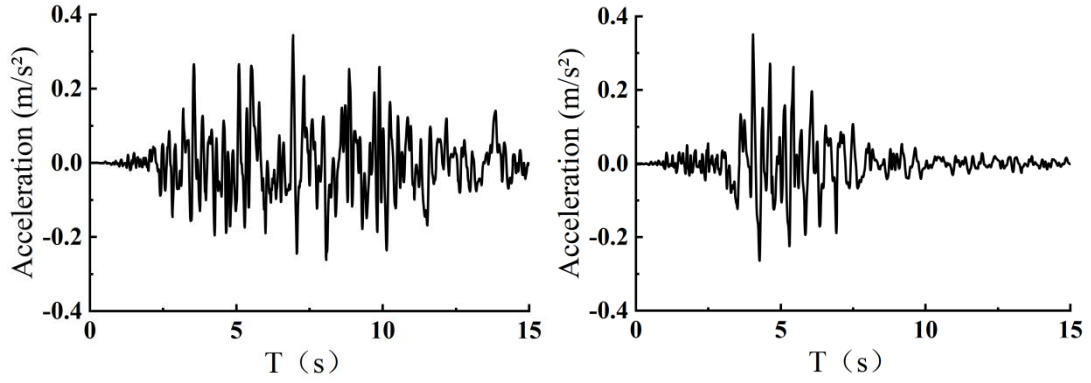

(a) Acceleration Time-History Curve of Kobe Seismic Wave (b) Acceleration Time-History Curve of Friuli Seismic Wave

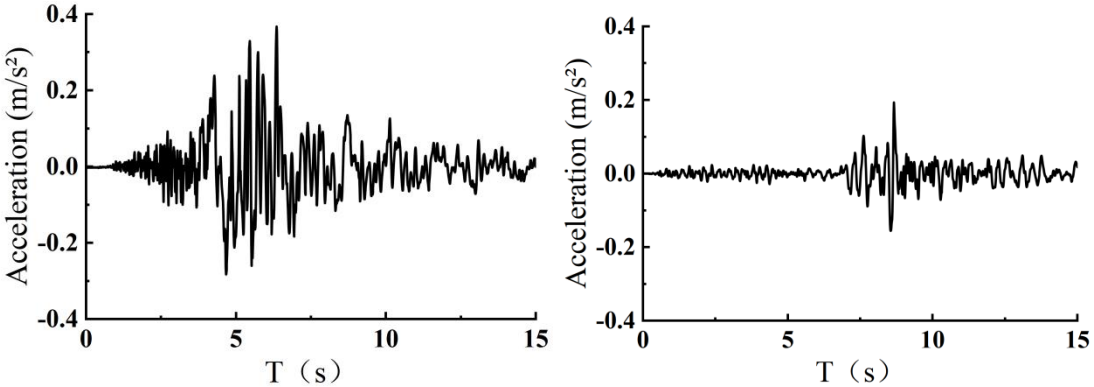

(c) Acceleration Time-History Curve of Loma Prieta Seismic Wave (d)Acceleration Time-History Curve of Trinidad Seismic Wave

Figure 2: Acceleration Time-History Curves of Four Different Selected Ground Motion Input Records

3. Results and Analysis

The monitoring points selected for the three-story building structure are shown in the Figureure, with Monitoring Point A positioned on the foundation surface to represent ground-mounted seismometer placement, and Monitoring Point B located 0.3 m above the foundation on the wall to simulate wall-mounted seismometer installation. By calculating the seismic responses of the three-dimensional soil-foundation-residential building system under vertical incidence of four earthquake waves with distinct spectral characteristics, acceleration time-history curves for Points A and B were obtained. Fourier transform was applied to these acceleration time histories to derive corresponding acceleration Fourier spectra, followed by computation of structural acceleration response spectrum curves. Comparative analysis of acceleration time histories, response spectra, and Fourier spectra between free-field conditions (without structure) and structural conditions (with building) was conducted to investigate seismic responses at monitoring points under different earthquakes. The computational results for internal monitoring Points A and B are illustrated in Figure. 3.

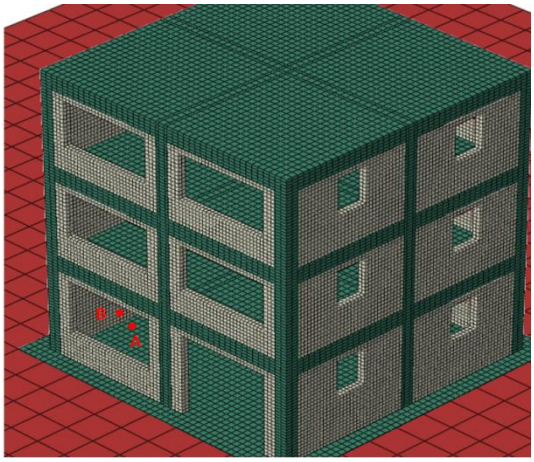

Figure 3: Selected Positions of the Monitoring Points within the Building

3.1 Peak Ground Motion and Spectral Analysis

The acceleration time-history curves, acceleration response spectra, and acceleration Fourier spectra of the four seismic ground motions are shown in Figure. 2, with their energy predominantly concentrated near the structural fundamental frequency in the simulated model. Monitoring points for the three-story building structure are illustrated in the Figureure: Monitoring Point A on the foundation surface represents ground-mounted seismometer placement, while Monitoring Point B, located 0.3 m above the foundation on the wall, simulates wall-mounted installation. Acceleration time histories at Points A and B were obtained through seismic response calculations under vertically incident SV waves with varying spectral characteristics. Fourier transforms and response spectrum analyses were performed on these time histories. Comparative analysis of acceleration time histories, response spectra, and Fourier spectra between structural and free-field conditions revealed significant peak acceleration deviations. Relative errors between structural and free-field peak accelerations (Table 4) demonstrated amplification (1.805% at A, 2.802% at B) under the Loma Prieta earthquake and attenuation (7.3% average) under the Trinidad earthquake, indicating soil-structure interaction effects depend on ground motion characteristics. Structural responses predominantly exhibited attenuation (equivalent shear wave velocity: 156 m/s in soft soil layers). Acceleration response spectra comparisons (Figure. 4) showed amplification within 0.25–0.6 s periods and attenuation above 15 Hz, consistent with the structure's dynamic properties.

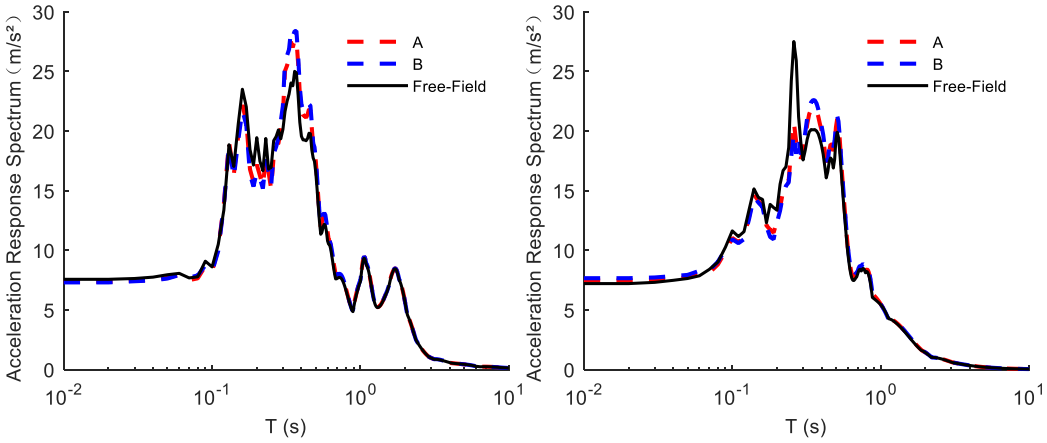

(a)Kobe Seismic Wave Earthquake (b)Friuli Earthquake

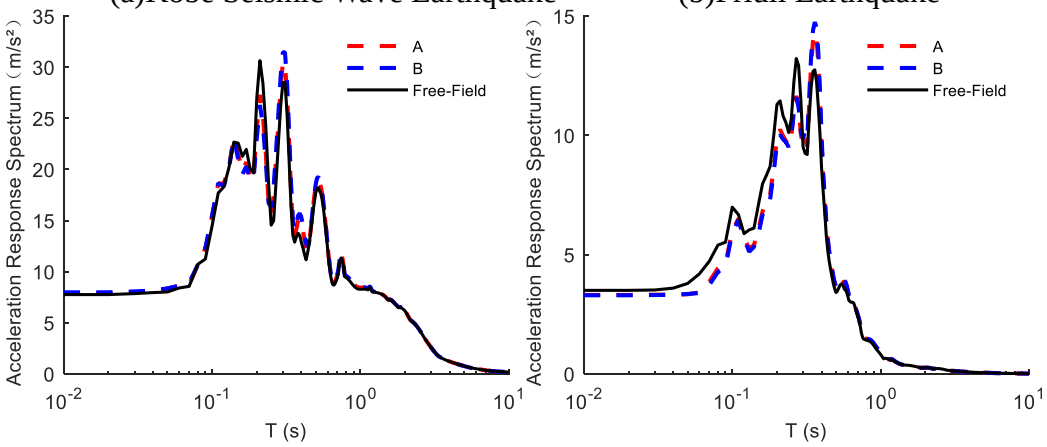

(c)Loma Prieta Earthquake (d)Trinidad Earthquake

Figure 4: Comparison Diagram of Responses between Monitoring Points Inside the Building and Free Ground Surface under Different Seismic Waves

Table 4: Maximum Response Values of Monitoring Points of the Three-story Frame Structure under Different Seismic Waves

Seismic Wave	A_{FF} (m/s²)	A_{SSI-A} (m/s²)	A_{SSI-B} (m/s²)	$\frac{(A_{SSI-A}-A_{FF})}{A_{FF}}$(%)	$\frac{(A_{SSI-B}-A_{FF})}{A_{FF}}$(%)
Kobe	7.574	7.368	7.315	-2.802	-3.540
Friuli	7.214	6.995	6.934	-3.142	-4.039
The Loma Prieta	7.760	7.902	7.983	1.805	2.802
The Trinidad	3.546	3.310	3.297	-7.128	-7.550

The comparison of acceleration Fourier spectra and acceleration response spectra under different seismic wave incidences reveals significantly greater structural responses near the building's fundamental frequency compared to the free field. The fundamental frequency of the three-story frame structure decreased from 4.23 Hz to 3.23 Hz, indicating a notable reduction in natural frequency due to the soft soil layers. To evaluate frequency-dependent response variations, acceleration Fourier spectral amplification coefficient comparisons were plotted (Figure. 5). The structure exhibited similar acceleration transfer functions across all four ground motions, with pronounced amplification near its natural frequency. The peak amplification coefficient at Monitoring Point A (1.2) was slightly lower than at Point B (1.25), correlating with the relative stiffness between the superstructure and soil layers—amplification effects intensified as the relative

stiffness approached unity (i.e., minimized stiffness contrast). Statistical analysis of peak amplification coefficients yielded average values of 1.2 (Point A) and 1.25 (Point B). Above 15 Hz, structural accelerations were significantly attenuated, attributable to high-frequency filtering effects enhanced by soil-structure interaction in soft soil layers with lower shear wave velocities.

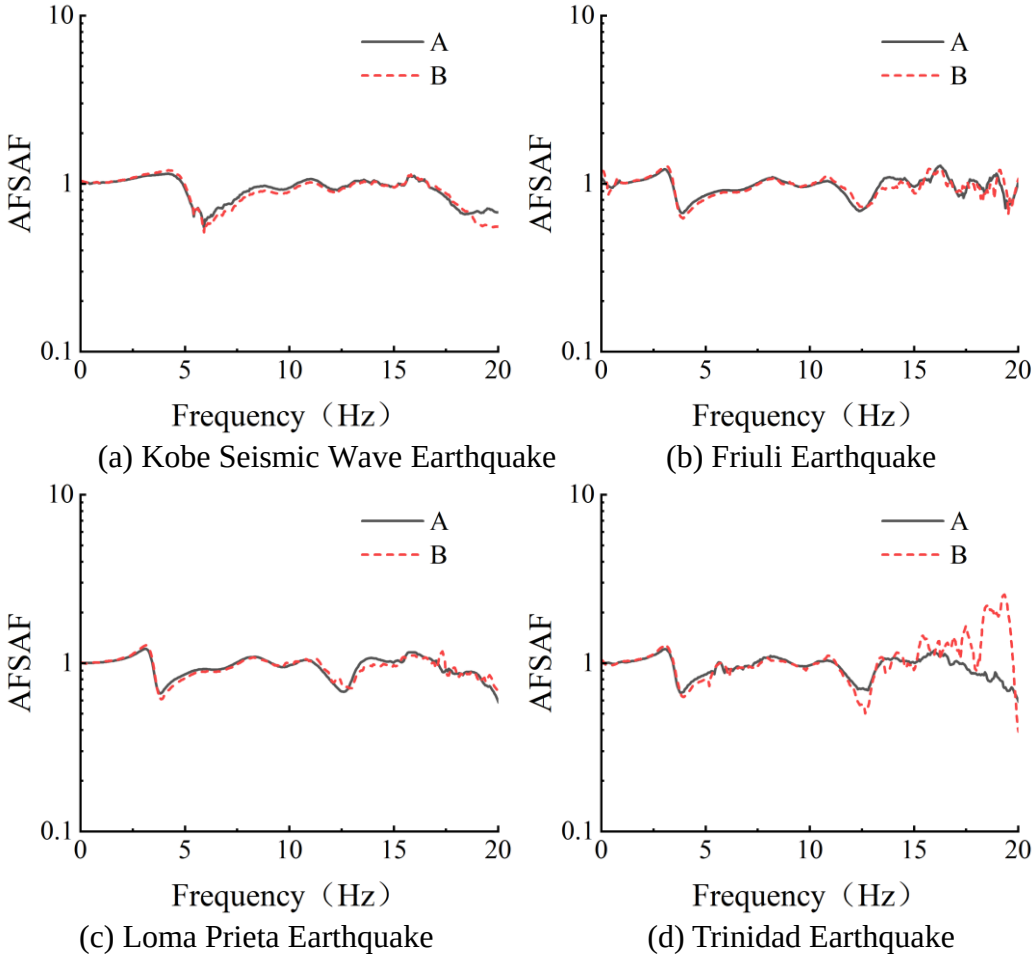

(a) Kobe Seismic Wave Earthquake (b) Friuli Earthquake

(c) Loma Prieta Earthquake (d) Trinidad Earthquake

Figure 5: Fourier Amplification Coefficients of Accelerations at Monitoring Points within Buildings under Different Seismic Waves

3.2 Instrumental Intensity Analysis

The instrumental intensity values were analyzed for finite element simulation data using the current Chinese intensity calculation method. The relationship between instrumental intensity, peak ground acceleration (PGA), and peak ground velocity (PGV) in the seismic intensity calculation code is defined as follows:

$$I_A = 3.17 \times \log_{10}(PGA) + 6.59 \tag{1}$$

$$I_v = 3.00 \times log_{10}(PGV) + 9.77 \tag{2}$$

The final seismic intensity$I_I$is determined by:

$$I_I = \begin{cases} I_v & I_A \geq 6.0 \; and \; I_v \geq 6.0 \\ (I_A + I_v)/2 & I_A < 6.0 \; or \; I_v < 6.0 \end{cases} \tag{3}$$

Table 5 presents the instrumental intensity deviations calculated from the acceleration time-history curves of the free-field surface and structural monitoring Points A and B under the four

seismic waves. The differences between the intensity values recorded within the building structure and those from the free-field surface are generally less than one degree, with maximum and minimum deviations of 0.192 and 0.026 degrees, respectively. Such deviations are within acceptable limits for post-earthquake instrumental intensity mapping, indicating that structural presence minimally impacts intensity assessments compared to free-field conditions. Acceleration differences induced by soil-structure interaction do not cause significant deviations in Chinese code-based intensity calculations, as all values remain within reasonable bounds.

Table 5: Deviation between the Structural Seismic Intensity Values Simulated and Calculated and the Seismic Intensity Values of the Free Ground Surface

Seismic Intensity Value Deviation	A	B
Kobe	-0.163	-0.192
Friuli	0.026	0.035
TheTrinidad	0.054	0.061
The Loma Prieta	0.027	0.032

4. Conclusions

The building types and installation methods of seismometers at general stations in the Ya'an region were used as the basis for selecting the superstructure in the integrated soil-structure interaction finite element model. By establishing a three-story reinforced concrete frame structure model on soft soil to simulate residential buildings housing seismometers in practical engineering, four actual ground motion records were selected as seismic inputs. The seismic responses of the structure under vertically incident SV waves were calculated, and the acceleration time histories, Fourier spectra, and acceleration response spectra from surface monitoring points were extracted. These results were compared with free-field (non-structural) spectra to analyze the influence patterns of ground motion within the structure. The study yielded the following conclusions:

(1) The differences in acceleration peaks between the two monitoring points (foundation and 30 cm above the foundation on the wall) are minimal, which is related to the increased overall stiffness of the structure due to masonry infill walls, resulting in smaller acceleration variations at lower building heights. However, significant differences in acceleration peaks are observed when compared to free-field recordings.

(2) Under different ground motions, soil-structure interaction (SSI) may either amplify or attenuate the acceleration response of the superstructure.

(3) The period range of amplified acceleration response spectra (0.2–0.6 s) correlates with the characteristics of the superstructure. The three-story residential building amplifies seismic responses within this range.

(4) Within the structure’s natural frequency range, the acceleration response is amplified by approximately 1.25 times, as shown by the transfer function between the structure and free field. Responses are attenuated at frequencies above 15 Hz, with soft soil layers intensifying the high-frequency filtering effects of SSI on ground motion recordings.

(5) Instrumental intensity deviations are closely related to input ground motion characteristics, site conditions, and structural properties. SSI has a minor influence on instrumental intensity under Chinese code specifications.

References

[1] Liu Y H, Song J D, Li Y S. ShakeAlert: development of the United States West Coast earthquake early warning system[J]. Earthquake Engineering and Engineering Dynamics, 2020,40(06): 61-70.

[2] Bao Y T, Wang P X, Xu M C, et al. Current status and latest progress of Japan's earthquake early warning system[J]. World Earthquake Engineering, 2024,40(03): 72-82.
[3] Li F. Construction of general stations for seismic intensity rapid reporting and early warning based on communication base stations[J]. Modern Transmission, 2023(3): 69-72.
[4] CAMPBELL K W. Effects of site characteristics on near-source recordings of strong ground motion[C]//. Workshop on Site-Specific Effects of Soil and Rock on Ground Motion and the Implications for Earthquake-Resistant Design, Santa Fe, NM, USA, 1983.
[5] STEWART J P, SEED R B, FENVES G L. Seismic Soil-Structure Interaction in Buildings. II: Empirical Findings [J]. 1999,125(1): 38-48.
[6] PANDEY B H, LIAM FINN W D, VENTURA C E. Modification of Free-Field Motions by Soil-Foundation-Structure Interaction for Shallow Foundations[C]//. Proc. of 15th World Conference on Earthquake Engineering, Lisbon, 2012.
[7] SOTIRIADIS D, KLIMIS N, MARGARIS B, et al. Influence of structure–foundation–soil interaction on ground motions recorded within buildings[J]. Bulletin of Earthquake Engineering, 2019,17(11): 5867-5895.
[8] SOTIRIADIS D, KLIMIS N, MARGARIS B, et al. Analytical expressions relating free-field and foundation ground motions in buildings with basement, considering soil-structure interaction[J]. Engineering Structures, 2020,216: 110757.
[9] SOTIRIADIS D, KLIMIS N, MARGARIS B, et al. Improved correlation between foundation and free-field ground motions through strong motion recordings and kinematic soil–structure interaction analyses[J]. Earthquake Engineering & Structural Dynamics, 2022,51(4): 725-743.
[10] NTINALEXIS M, BOMMER J J, RUIGROK E, et al. Ground-motion networks in the Groningen field: usability and consistency of surface recordings[J]. Journal of Seismology, 2019,23(6): 1233-1253.
[11] Zhou B F, Song Q, Ren Y F, et al. The Study on the Influence and Application of Foundation Pier Height on Strong Motion Records[J]. Earth Science, 2024,49(2): 414-424.
[12] LIANG J, FU J, TODOROVSKA M I, et al. Effects of site dynamic characteristics on soil–structure interaction (II): Incident P and SV waves[J]. Soil Dynamics and Earthquake Engineering, 2013,51: 58-76.
[13] Liang Y W, Yang L J, Han Bet al. Effects of the soil nonlinearity on dynamic soil-structure interaction:A case study of Millikan library building[J]. Earthquake Engineering and Engineering Dynamics, 2022,42(3): 10.
[14] PITILAKIS K D, KARAPETROU S T, FOTOPOULOU S D. Consideration of aging and SSI effects on seismic vulnerability assessment of RC buildings[J]. Bulletin of Earthquake Engineering, 2014,12(4): 1755-1776.
[15] KARAPETROU S T, FOTOPOULOU S D, PITILAKIS K D. Seismic vulnerability assessment of high-rise non-ductile RC buildings considering soil–structure interaction effects[J]. Soil Dynam Earthq Eng, 2015,73: 42-57.
[16] CAVALIERI F, CORREIA A A, PINHO R. Variations between foundation-level recordings and free-field earthquake ground motions: numerical study at soft-soil sites[J]. Soil Dynamics and Earthquake Engineering, 2021,141: 106511.
[17] Liu J B, Wang Z Y, Du X L, et al. Three-dimensional visco-elastic artificial boundaries in time domain for wave motion problems[J]. Engineering Mechanics, 2005,22(6): 46-51.